# Determining the In-Plane Orientation and Binding Mode of Single Fluorescent Dyes in DNA Origami Structures

Kristina Hübner, Himanshu Joshi, Aleksei Aksimentiev, Fernando D. Stefani,\* Philip Tinnefeld,\* and Guillermo P. Acuna\*



Downloaded via UNIV ILLINOIS URBANA-CHAMPAIGN on April 2, 2021 at 18:36:01 (UTC). See https://pubs.acs.org/sharingguidelines for options on how to legitimately share published articles.

Cite This: ACS Nano 2021, 15, 5109-5117



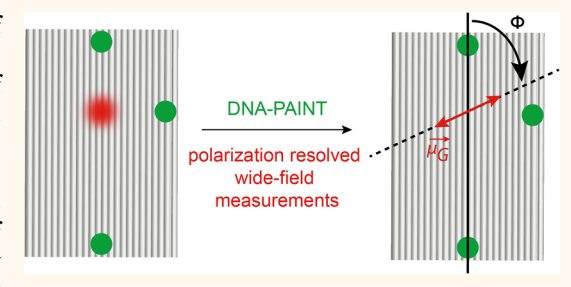
**ACCESS** I

III Metrics & More

Article Recommendations

s Supporting Information

ABSTRACT: We present a technique to determine the orientation of single fluorophores attached to DNA origami structures based on two measurements. First, the orientation of the absorption transition dipole of the molecule is determined through a polarization-resolved excitation measurement. Second, the orientation of the DNA origami structure is obtained from a DNA-PAINT nanoscopy measurement. Both measurements are performed consecutively on a fluorescence wide-field microscope. We employed this approach to study the orientation of single ATTO 647N, ATTO 643, and Cy5 fluorophores covalently attached to a 2D rectangular DNA origami structure with different



nanoenvironments, achieved by changing both the fluorophores' binding position and immediate vicinity. Our results show that when fluorophores are incorporated with additional space, for example, by omitting nucleotides in an elsewise double-stranded environment, they tend to stick to the DNA and to adopt a preferred orientation that depends more on the specific molecular environment than on the fluorophore type. With the aid of all-atom molecular dynamics simulations, we rationalized our observations and provide insight into the fluorophores' probable binding modes. We believe this work constitutes an important step toward manipulating the orientation of single fluorophores in DNA origami structures, which is vital for the development of more efficient and reproducible self-assembled nanophotonic devices.

**KEYWORDS:** DNA nanotechnology, super-resolution microscopy, DNA-PAINT, single-molecule fluorescence, polarization-resolved microscopy

he DNA origami technique is revolutionizing nanofabrication by molecular self-assembly because it provides control and versatility to organize different molecules and nanoparticles in well-defined geometric arrangements. In particular, this technique has proven extremely useful to fabricate nanophotonic devices with specific functions by setting single-photon emitters (SPEs), such as fluorescent molecules or quantum dots, and metallic nanoparticles (MNPs) in precise geometries with high positional and stoichiometric control.<sup>2-4</sup> In some cases, DNA origami structures are used to host solely MNPs like in chiral plasmonic structures<sup>5-7</sup> or DNA sensors based on circular dichroism. 8,9 In others, only SPEs are organized, such as in multichromophoric Förster resonance energy transfer (FRET) chains capable of transporting optical excitations 10-13 or FRET-based DNA sensors. 14,15 Finally, DNA origami structures have also been used to construct more complex hybrid nanostructures, where SPEs and MNPs acting as optical nanoantennas (OAs) were combined to enhance the interaction of molecules with light. Examples include OAs for enhanced fluorescence 16-18 or Raman 1

spectroscopy, plasmon-assisted FRET,<sup>23,24</sup> strong-coupling at room temperature,<sup>25,26</sup> and directional emission.<sup>27,28</sup>

Importantly, the efficiency of nanophotonic devices depends not only on the relative position of their components but also on their relative orientation. For example, in order to form a directional OA, two or more nanorod elements must be placed side-by-side in a parallel fashion. Similarly, the efficiency of dipole—dipole interactions between two fluorophores (FRET) depends, among several factors, on the relative orientation of the fluorophores through the  $\kappa^2$  factor. This factor ranges from 0 (for perpendicular transition dipoles) to the maximum value of 4 when their transition dipoles are aligned. Regarding the

Received: December 8, 2020 Accepted: February 25, 2021 Published: March 4, 2021





interaction between optically active molecules and OAs, the effect is 2-fold. The molecular excitation rate is proportional to  $\langle \vec{E} \cdot \vec{\mu}_{\rm G} \rangle^2$ , with  $\vec{\mu}_{\rm G}$  the absorption transition dipole moment of the molecule and  $\vec{E}$  the electric field at the molecule's position arising from the sum of the incident field and the field induced by the OA. The molecular radiative decay rate also depends on the relative orientation between the emission transition dipole moment  $\vec{\mu}_{\rm E}$  and the OA, leading to a wide range of effects, from strong enhancement to virtually complete suppression of photon emission.  $^{27,33-35}$ 

So far, various protocols have been introduced to incorporate anisotropic MNPs, such as gold nanorods<sup>36</sup> and triangular plates,<sup>37</sup> in DNA origami structures with positional and orientational control. In contrast, while the DNA origami technique routinely enables the assembly of molecules with high positional accuracy, controlling the orientation of single molecules remains challenging. Basically, there are two kinds of strategies to incorporate molecules into DNA origami structures. The first one is the well-known, noncovalent binding to double-stranded DNA (dsDNA) helices. This approach offers orientational control because different molecules bind differently to the dsDNA structure, depending on the chemical structure. Some bind preferentially in between bases (intercalators); others bind to the minor or major groove (groove binders), or externally along the dsDNA chain.<sup>38</sup> Gopinath et al.39 reported an example of this approach, labeling DNA origami structures with the intercalating dye TOTO-3, which forms an angle of  $70^{\circ} \pm 10^{\circ}$  between  $\overrightarrow{\mu}_{C}$  and the dsDNA helix. Unfortunately, this level of orientational control<sup>40</sup> comes at the expense of losing stoichiometric and positioning control as it is not possible to predefine the positions nor the number of binding molecules.

The second strategy to incorporate molecules into a DNA origami structure consists of attaching them covalently to specific constituent single-stranded DNA (ssDNA) staples, 41 at either the 5'- or 3'-ends, or internally, using, for example, an amino-C6 linker. This approach provides high positional and stoichiometric control to incorporate molecules in DNA origami structures. 10 However, in contrast to the case of DNA binding molecules, the resulting orientation of molecules is not yet predictable. This is due, in part, to the complexity of the interaction between small molecules and DNA which depends not only on the molecular identity but also on the type of linker and the surrounding environment. <sup>24</sup> Also, no method of general applicability has been available to reliably determine the orientation of single molecules with respect to DNA origami structures. Earlier works have addressed the orientation of fluorophores linked to DNA using FRET. 42-45 For example, it was found that Cy3 and Cy5 dye molecules attached to dsDNA maintain a preferential orientation when linked via a threecarbon linker due to blunt end sticking 46 but present a high degree of rotational freedom when other linkers are used. 45 FRET measurements have the advantage that they can be conducted at the single-molecule level, but they do not address the orientation of fluorophores with respect to the DNA structure. Instead, they report on the relative orientation between donor and acceptor molecules, and that measurement relies strongly on an accurate determination of the donoracceptor separation distance. More recently, the position and orientation of single molecules attached to short dsDNA chains were determined through single-molecule localization techniques. 47-49 Because the dsDNA chains were shorter than the

persistence length, they could be considered rectilinear, and the relative orientation of the fluorophores with respect to the dsDNA could be inferred at the cost of the DNA being physically adsorbed to a positively charged surface.

Here, we present a technique of general applicability to study the orientation of single fluorescent molecules in DNA origami structures. It is based on two independent measurements that can be performed consecutively on surface-immobilized DNA origami structures using a wide-field fluorescence microscope. First, a polarization-resolved excitation measurement is used to determine the 2D orientation of the target fluorescent molecules. Second, a super-resolution (nanoscopy) measurement using the DNA-PAINT technique<sup>50</sup> is used to retrieve the orientation of the DNA origami "host" structure. The DNA origami hosts the dsDNA that the dyes are bound to in a fixed horizontal orientation while maintaining its physiological buffer environment. With this technique, we initially determined the orientation of single ATTO 647N molecules covalently attached to a rectangular DNA origami structure in three configurations with different expected nanoenvironments. For every case, the ATTO 647N delivered a nearly Gaussian distribution of orientations with a distinct mean orientation. Then, we performed analogous experiments with ATTO 643 and Cy5 fluorophores for two configurations in order to determine the hierarchy between the two main factors that affect the final orientation: nanoenvironment and fluorophore identity. Finally, using molecular dynamics simulations, we assigned the observed orientations to molecular structures and interactions that are likely related to the true conformations. Overall, these results enable the design and fabrication of highly efficient nanophotonic devices by self-assembly using DNA origami structures, where SPEs could be set not only with high positional and stoichiometric control but also with orientational control.

### **RESULTS AND DISCUSSION**

A schematic of the sample employed is shown in Figure 1a. It consists of a 2D rectangular DNA origami structure (85 nm × 71 nm) based on 24 helices with different modifications. A single ATTO 647N, ATTO 643, or Cy5 molecule (indicated by a red spot in Figure 1a) was covalently attached to a defined base of an ssDNA staple through a single C6-linker. For the DNA-PAINT measurements, we further extended 18 ssDNA staples with an 11-nucleotide sequence to form three binding sites (green spots in Figure 1a, top view), arranged in an asymmetric pattern. In order to immobilize the samples onto glass coverslips, six biotinylated ssDNA staples are incorporated into the DNA origami structure (blue spots in Figure 1a, bottom view) on the hereafter defined underside of the DNA origami structure.

The ATTO 647N fluorophore was selected not only for its brightness and photostability but also because it is moderately hydrophobic, carries a net electrical charge of +1, and tends to stick to surfaces and DNA. This sticking can be hydrophobic, due to an interaction with the hydrophobic core of the DNA, or electrostatic, due to an interaction with the negatively charged DNA phosphate backbone. ATTO 643 is a hydrophilic version of the ATTO 647N and shows a reduced tendency for unspecific sticking. The Cy5 fluorophore is a member of the group of cyanine dyes and carries a net charge of +1. In this work, we want to address the question of whether fluorophores show preferential binding sites depending on the position and motional freedom within the DNA origami structure. To this end, we prepared three samples where a single fluorophore is linked in different ways to the DNA origami structure, always

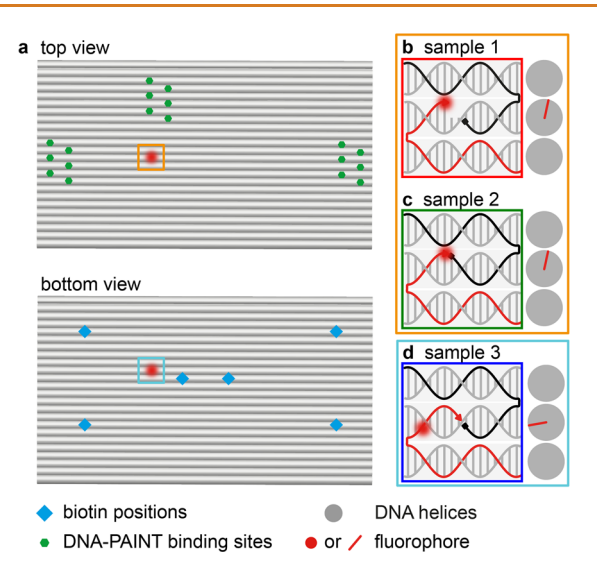


Figure 1. (a) Sketch of the top and bottom view of the rectangular DNA origami structure including different modifications: 6 biotins (blue), a single fluorophore (ATTO 647N, ATTO 643, or Cy5; red), and 18 DNA sequences (green) forming three binding sites for DNA-PAINT measurements in an asymmetric pattern. (b-d) Inset of the DNA helical winding highlighting the position of the ssDNA staple (red line) labeled with the fluorophore (red spot), the adjacent ssDNA staple (black line), and the scaffold strand (gray line) for the three samples employed.

covalently attached but with different local environments. In samples 1 and 2, the fluorophore (highlighted with an orange square in the top view of Figure 1a) is linked at the same position in the helix, facing toward the neighboring helix (Figure 1b,c). This is achieved through a modification at the 3'-end of the corresponding ssDNA staple (Supporting Information, Figure S1a). The difference between these samples is that in sample 1

the next adjacent ssDNA staple after the fluorophore modification is shortened by two nucleotides (Figure 1b), whereas in sample 2 the adjacent ssDNA staple is not shortened (Figure 1c). Thus, the fluorophore is expected to have more freedom to find a favorable position in sample 1. In sample 3, the fluorophore (highlighted by a blue square in the bottom view of Figure 1a) is incorporated at a different position using an internal modification of an ssDNA staple in a different helix (Supporting Information, Figure S1b) so that the fluorophore is facing toward the underside of the DNA origami structure (Figure 1d). Samples 1 and 2 were prepared for all three fluorophores (ATTO 647N, ATTO 643, and Cy5) whereas sample 3 was solely fabricated with a single ATTO 647N fluorophore.

Measurements were performed in a home-built wide-field microscope equipped with both green (532 nm) and red (644 nm) lasers for fluorescence excitation. The polarization-resolved measurements were carried out under epifluorescence illumination, by stepwise rotating the linear polarization of the red laser excitation by 20° every five seconds. This procedure was repeated 18 times to cover twice an excitation polarization range of 180°. An example fluorescence trace showing a periodic intensity modulation is shown in Figure 2a. This modulation can be quantified as  $M=rac{I_{\max}-I_{\min}}{I_{\max}+I_{\min}}$ , with  $I_{\max}$  and  $I_{\min}$  the highest and lowest intensity values extracted from each trace, respectively. Histograms showing the distributions of the modulation for all samples and fluorophores are included in the Supporting Information in Figure S2. We only considered single-molecule traces showing a significant modulation  $^{47}$  (i.e., M > 0.15) in order to exclude samples in which the fluorophore is relatively free to rotate and thus cannot be studied with the forthcoming analysis. Table S1 includes the number of traces studied and the fraction that met this condition for each sample and fluorophore.

For the traces with M > 0.15, we attribute the excitation

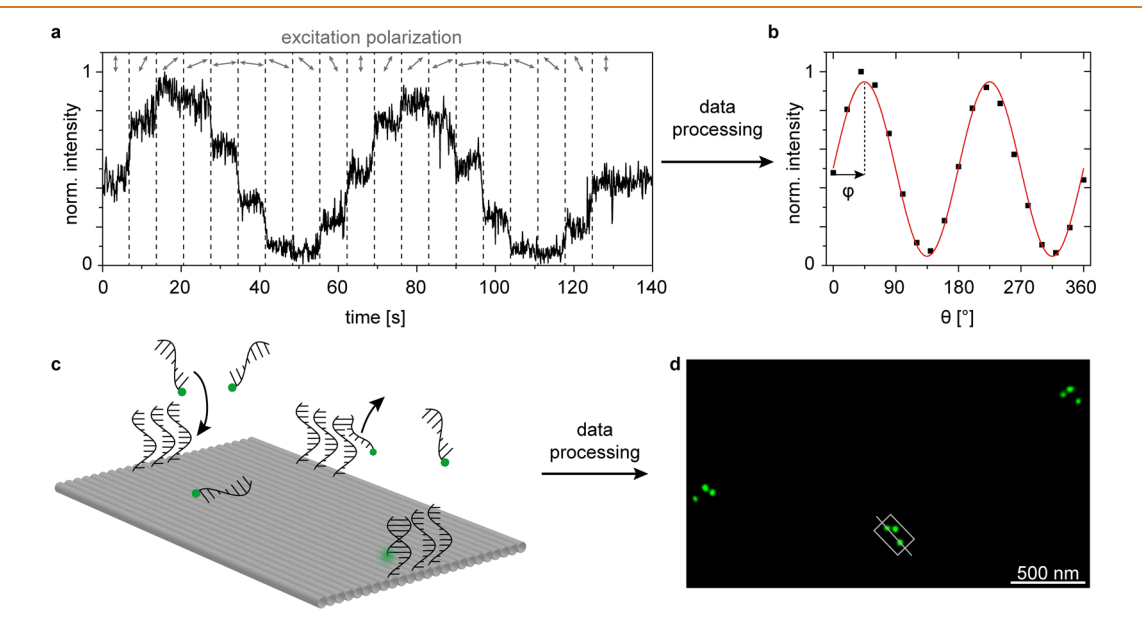


Figure 2. (a) Polarization-resolved excitation measurements. Exemplary ATTO 647N fluorescence trace obtained by rotating the incident polarization angle  $(\theta)$  by 20° every five seconds. (b) Mean fluorescence intensity vs  $\theta$  together with a  $\cos^2$  fit to obtain the in-plane orientation  $(\varphi)$  of the excitation transition dipole moment  $\overrightarrow{\mu}_G$  with respect to the microscope. (c) DNA-PAINT nanoscopy measurements. Sketch of the binding and unbinding of the imager strands labeled with a single ATTO 542 onto the DNA-PAINT binding sites. (d) Super-resolved DNA-PAINT image corresponding to three DNA origami structures showing the asymmetric triangular pattern. Based on this image, the orientation in 2D as well as the binding geometry (upright or upside down) of each DNA origami (gray rectangle) can be extracted (gray line).

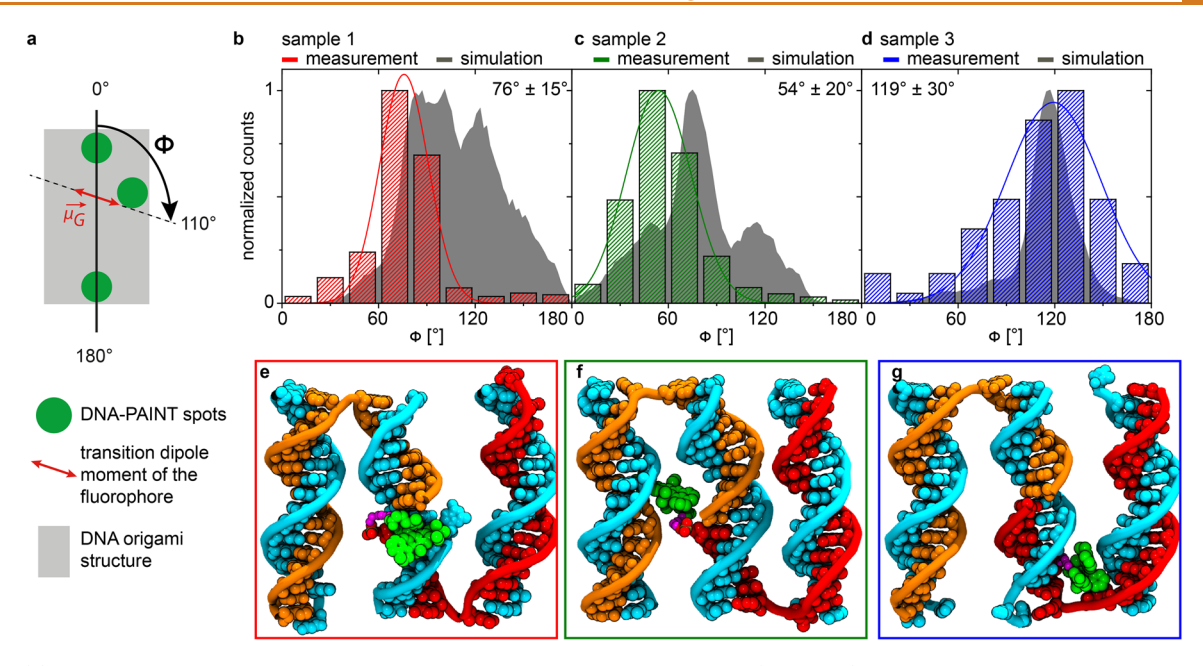


Figure 3. (a) Coordinate system employed to estimate the angle  $\phi$  that the fluorophore (i.e., its  $\overrightarrow{\mu}_{\rm G}$ ) forms with the DNA origami host structure. (b-d) Distributions of  $\phi$  for ATTO 647N on the three samples obtained experimentally (bars) and from all-atom MD simulations (shaded gray curves). The experimental distributions are fitted with a Gaussian function; its mean value and the standard deviation are shown next to the plot. Each simulation histogram shows data from two independent runs, 1  $\mu$ s long, sampled every 20 ps. (e-g) Conformations of ATTO 647N from all-atom MD simulations corresponding to the average experimental orientation of the three samples. The ATTO 647N is shown in green, the staple strand carrying the ATTO 647N in red, and the C6-linker in magenta, and the adjacent staple and scaffold strands are shown in orange and blue, respectively.

modulation to fluorophores spending a considerable fraction of the time bound to the DNA origami structure. For each polarization, the mean intensity was extracted and plotted against the incident polarization angle  $\theta$ . The resulting intensity vs  $\theta$  curve was fitted to a  $\cos^2(\theta-\varphi)$  function, as shown in Figure 2b. The obtained value of  $\varphi$  corresponds to the in-plane orientation of the fluorophore's absorption transition dipole moment,  $\overrightarrow{\mu}_G$ .

Next, we performed DNA-PAINT imaging by adding a solution containing 3 nM 7-nucleotide ssDNA sequences (imager strands) labeled with a single ATTO 542 dye (Figure 2c). Every transient binding of an imager strand to one of the three binding sites leads to a fluorescence spot on the camera image which is used to precisely localize the binding site. The reconstructed super-resolved images reveal the triangular asymmetric pattern of each DNA origami structure (Figure 2d), which not only provides the orientation of each DNA origami rectangle on the glass coverslip but also shows whether it was immobilized upright or upside down (for further information, see Figure S3). For this 2D DNA origami, the structure can self-assemble with the biotin modifications ending on the "upper-side" as previously reported. 53,54 We determined that approximately 33% of all the DNA origami structures studied were bound to the glass coverslip with the "upper-side" facing toward the glass surface. This does not affect our analysis, as shown in Figure S4 of the Supporting Information.

By combining both sets of measurements, we obtained the angle of each fluorophore  $(\overrightarrow{\mu}_{\rm G})$  with respect to the dsDNA helix of its host DNA origami structure. We called this angle  $\phi$ , defined according to the coordinate system shown in Figure 3a. Figure 3b–d shows the distributions of  $\phi$  obtained for the three samples labeled with a single ATTO 647N. Based on a Gaussian fit to each distribution, the mean orientations are found to be  $\phi$ 

=  $76^{\circ} \pm 15^{\circ}$ ,  $54^{\circ} \pm 20^{\circ}$ , and  $119^{\circ} \pm 30^{\circ}$  for samples 1, 2, and 3, respectively. The distinct distributions of  $\phi$  reveal that the notorious stickiness of ATTO 647N to DNA strongly depends on the specific nanoenvironment. This is especially illustrated by a more than  $20^{\circ}$  difference in the average molecular orientation for samples 1 and 2, which differ only by two missing nucleotides in sample 1.

In order to rationalize these findings, we performed all-atom molecular dynamics (MD) simulations of the relevant threehelix fragments taken from the experimental DNA origami designs (see Figure 3e-g and Figure S5a). Two independent simulations, each 1  $\mu$ s long, were performed for each system (the videos from the simulations for each sample are included in the Supporting Information, movies S1, S2, and S3). From these simulations, we extracted the in-plane orientation of the fluorophore  $(\phi)$  at 20 ps time steps. The obtained distributions of  $\phi$  are additionally shown in Figure 3b-d (gray). For sample 3, we find an exquisite agreement between experiment and simulations. The broadening of the experimental data can likely be assigned to possible wobbling of the overall structure. On the other hand, samples 1 and 2 exhibit larger differences between experiment and simulation. Visual inspection of the simulation videos reveals that several, very different conformations of the dye within the DNA origami structure are visited for relatively long times indicating that the energy landscape might be too rugged to allow for a representative sampling of all possible conformations within the time scale accessible to the simulations. Vice versa, by searching in the simulations for conformations that match the experimental  $\phi$ -values, we extracted conformations that are likely to be visited for longer times in the experiments (alternative conformations representing different subpopulations of the simulations are shown in Figure S5e).

A great finding arises from the comparison of the results obtained with sample 1 and 2, that only differ by two missing nucleotides in sample 1. Interestingly, the simulated conformations of sample 1 with  $\phi$ -values matching the experiments are characterized by intercalation of the dye at the position of the two missing nucleotides (see representative structure in Figure 3e). In contrast, for sample 2, the subpopulation of the simulation with the  $\phi$ -values matching the experimental average distinguishes itself by the interaction of the dye with the neighboring helix (see representative structure in Figure 3f). In analogy, we also extracted a representative conformation of sample 3 (Figure 3g) that reveals potential reasons for the better agreement of experiment and simulation. For sample 3, the dye is located closer to a crossover of a neighboring helix which creates a preferential binding pocket (Figure 3g).

In addition, we performed measurements on samples 1 and 2 with single ATTO 643 and Cy5 fluorophores. The measured distributions of  $\phi$  are shown in Figure 4, where the previous

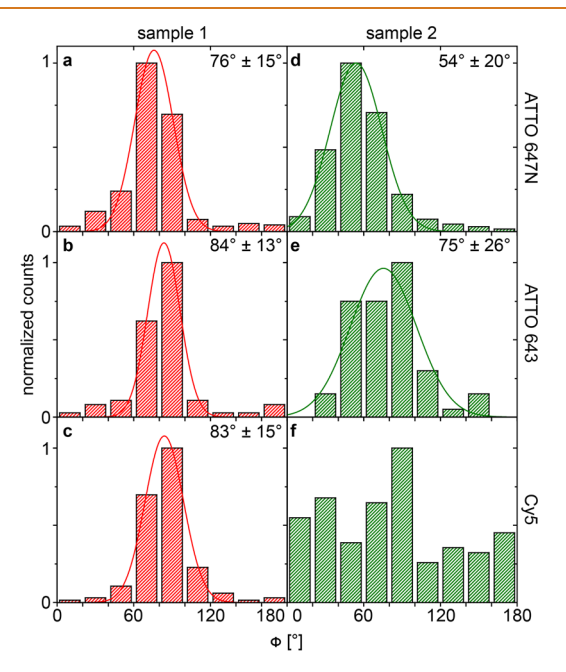


Figure 4. Distributions of  $\phi$  for ATTO 647N, ATTO 643, and Cy5 fluorophores incorporated in the DNA origami structure in samples 1 and 2. The curves are fits to a Gaussian function; the mean and standard deviations are shown next to the plots.

results for ATTO 647N are added for comparison. For sample 1, narrow distributions of  $\phi$  were obtained for every fluorophore characterized by similar mean values of  $76^{\circ} \pm 15^{\circ}$ ,  $84^{\circ} \pm 13^{\circ}$ , and  $83^{\circ} \pm 15^{\circ}$  for ATTO 647N, ATTO 643, and Cy5, respectively. Also, for this sample, the fraction of traces showing a modulation M > 0.15 was larger than 90% for the three dyes. In contrast, for sample 2, broader distributions of  $\phi$  were measured with more dissimilar mean values of  $54^{\circ} \pm 20^{\circ}$  and  $75^{\circ} \pm 26^{\circ}$  for ATTO 647N and ATTO 643, respectively. For Cy5, the obtained distribution of  $\phi$  in sample 2 was nearly uniform, indicating that Cy5 finds no preferential orientation under these conditions. Sample 2 also showed different behaviors in the fraction of modulating traces for the three fluorophores. While ATTO 647N and Cy5 show a considerably high fraction of modulating traces (61% and 88%, respectively), only 20% of the traces registered for ATTO 643 showed significant modulation. Similar to our simulations of the ATTO 647N systems, in our

simulations of the Cy5 dye-conjugated DNA constructs (Supporting Information, Figure S6 and Movies S4 and S5), the dye was observed to interact strongly with the unpaired DNA nucleotides in sample 1 and with the grooves of the DNA helices in sample 2. Overall, these results confirm that in sample 1 the fluorophores adopt similar orientations in the space left by the two missing nucleotides. In sample 2, without the extra available space, the fluorophore orients in a less defined manner with a stronger dependence on the fluorophore type.

# **CONCLUSION**

In summary, we have developed a technique to determine the inplane orientation of fluorescent molecules covalently attached to DNA origami structures. This technique combines a polarization-resolved excitation measurement and DNA-PAINT nanoscopy and can be implemented in wide-field fluorescence microscopes. We applied this approach to study the orientation of different fluorophores covalently incorporated into DNA origami structures in three different ways, each one generating a different local environment for the fluorophores. We showed that ATTO 647N, one of the most used dyes in single-molecule experiments, not only strongly sticks to DNA but also adopts preferential binding geometries depending on the local environment. MD simulations of the corresponding experimental systems showed that the local environment of a dye conjugated to DNA can qualitatively change the manner in which the dye interacts with the DNA and thereby affect the preferential orientation of the dye. Although we found the conformational sampling afforded by our brute-force MD simulations to be insufficient to quantitatively predict the preferential orientation of the dyes, the simulations nevertheless yielded substantial structural information to assign probable conformations for each sample studied and allow us to extract likely binding modes.

Importantly, we find that leaving extra space to a terminally attached fluorophore (e.g., by shortening the adjacent staple strand) leads to stronger binding and a narrower, more defined distribution of dye orientations. These findings were validated by experiments with three different fluorophores: ATTO 647N, ATTO 643, and Cy5. In contrast, an internally attached fluorophore in the DNA strand (sample 3) does not lead to a narrower distribution of orientations.

The dynamics of dye molecules around a DNA helix is governed by a complex interplay of electrostatic and hydrophobic interactions. This complexity imposes a considerable challenge for the accurate prediction of the final orientation of the molecules within a DNA origami structure. The experimental approach presented here should be applicable to other dyes and a variety of relevant samples using, *e.g.*, bisfunctional fluorescent dyes. Further measurements of molecular orientation, incorporating 3D techniques, <sup>5.5</sup> in combination with MD simulations, will enable the generation of sufficient empirical knowledge to finally predict and manipulate molecular orientation in DNA origami structures. This, in turn, will lead to much more efficient and reproducible self-assembled nanophotonic applications. <sup>56</sup>

# **METHODS**

**DNA Origami.** The rectangular DNA origami structure was designed using CaDNAno.<sup>57</sup> It is based on a 7249-nucleotide long scaffold extracted from a M13mp18 bacteriophage and folded into the desired rectangular shape with the help of 186 staples (see the SI, Section S6) mixed with a 10-fold excess of staples to scaffold. Unmodified staple strands were purchased from IDT; biotin-function-

alized staples as well as the dye labeled staple strands with ATTO 647N, ATTO 643, and Cy5 for sample 1 and 2 were purchased from Eurofins Genomics GmbH and for sample 3 with ATTO 647N from Biomers GmbH. The fluorophores used here are linked through a C6-linker to the single-stranded DNA either on the 3'-end in samples 1 and 2 (Figure S1a) or internally in sample 3 (Figure S1b). A temperature ramp is driven to self-assemble the scaffold and staple mixture to the designed rectangular DNA origami structure. The mixture first was heated to a temperature of 70 °C, where it stayed for 5 min; then, the temperature was decreased down to 24 °C following a ramp of 1 °C min-1. To get rid of the excess of staple strands, agarose gel electrophoresis is used as a purification method. To this end, a 1.5% agarose gel (Biozym LE agarose) containing ROTIGelStain (Roth) as an intercalating dye for DNA is made. Additionally, a 10× BlueJuice gel loading buffer (Thermo Fischer Scientific) is used to load the gel pockets with the unpurified DNA origami structures. The gel runs at 80 V for 90 min in a 0.5× TAE 11 mM MgCl<sub>2</sub> buffer, cooled in an ice water bath. After electrophoresis, the bands in the gel containing the DNA origami structure were cut out and squeezed with a glass slide to extract the purified DNA origami structures. The final concentration of the DNA origami structures was determined on a Nanodrop 2000 spectrophotometer (Thermo Fisher Scientific).

Surface Preparation and Immobilization. For surface immobilization, glass slides were rinsed with Milli-Q water and cleaned in a UV cleaning system (PSD Pro System, Novascan Technologies). After cleaning, two slides were glued together with double-sided adhesive tape forming a chamber between the two slides. The surface was passivated with BSA biotin (1 mg/mL, Sigma-Aldrich Chemie GmbH) and neutrAvidin (0.5 mg/mL, Sigma-Aldrich Chemie GmbH), both incubated for 15 min and washed with 1× PBS buffer after incubation. Then, the DNA origami structure can be immobilized in a buffer containing 12 mM MgCl<sub>2</sub> via biotins binding to the functionalized surface. For the fluorescence measurements, the buffer was exchanged to a buffer containing a reducing and oxidizing (ROX) system as well as oxygen scavenging agents in order to increase the photostability of the fluorophores. In particular, we used trolox/troloxquinone as the reducing and oxidizing system, in addition to glucose oxidase for oxygen removal in a 1× TAE buffer containing 2 M NaCl. 58,5

Wide-Field Setup. Measurements were performed on a home-built wide-field microscope based on an inverted Olympus IX71 microscope. For excitation, a 644 nm diode laser (ibeam smart, Toptica Photonics) and 532 nm fiber laser (MPB Communications) are used. Spectral clean-up of the lasers' emission is performed through the following filters: Brightline HC 650/13, Semrock (red range); and Z532/647x, Chroma (green range). After spectral cleaning, the laser is directed through a linear polarizer (LPVISC100-MP2 510-800 nm, Thorlabs) to clean up the polarization of the beam and a lambda half waveplate (AHWP05 M 400-800 nm, Thorlabs) mounted in a rotatable motorized stage (K10CR1/M stepper motor, Thorlabs). The laser is then focused on the back focal plane of the objective (UPLXAPO 100×, numerical aperture (NA) = 1.45, working distance (WD) = 0.13, Olympus). For sample stabilization, an actively stabilized optical table (TS-300, JRS Scientific Instruments) and a nosepiece stage (IX2-NPS, Olympus) are implemented. The emitted light is redirected through the objective and spectrally separated from the excitation laser by a dichroic beamsplitter (Dual Line zt532/640 rpc, AHF Analysentechnik). The fluorescence light is filtered by an emission filter in the red range (ET 700/75, Chroma) as well as in the green range (BrightLine 582/75, AHF Analysentechnik) and focused onto an EMCCD camera (iXon X3 DU-897, Andor). Data acquisitioning is performed by the open source microscopy imageJ software Micro-Manager.6

**Simulations.** All MD simulations were performed using program NAMD2, <sup>61</sup> a 2 fs integration time step, 2–2–6 multiple time stepping, periodic boundary conditions, and particle mesh Ewald (PME) method over a 1 Å resolution grid to calculate the long-range electrostatic interaction. <sup>62</sup> The Nosé–Hoover Langevin piston <sup>63</sup> and Langevin thermostat were used to maintain the constant pressure and temperature in the system. An 8–10–12 Å cutoff scheme was used to calculate van der Waals and short-range electrostatic forces. The SETTLE algorithm <sup>64</sup> was applied to keep water molecules rigid

whereas the RATTLE algorithm<sup>65</sup> constrained all other covalent bonds involving hydrogen atoms. CHARMM36 force field parameters described the bonded and nonbonded interactions among DNA water and ions.<sup>66</sup> The force-field parameters of the dye molecules (ATTO 647N and CyS) covalently conjugated with the C6 linker to DNA were obtained using the CHARMM General Force Field (CGenFF) web server.<sup>67</sup> We used custom nonbonded fix (NBFIX) corrections to improve the nonbonded interaction among DNA and ions.<sup>68</sup> The coordinates of the system were saved at an interval of 20 ps. Visualization, analysis, and postprocessing of the simulation trajectories were performed using VMD<sup>69</sup> and CPPTRAJ.<sup>70</sup>

We created three all-atom models of rectangular DNA origami systems corresponding to the three different dye modification used in experiments, namely, sample 1, 2, and 3. The CaDNAno design of the DNA origami plate was converted to an idealized all-atom representation using a previously described method. In order to create a realistic and smaller analogue of the DNA origami suitable for the all-atom simulations, we kept only a 15 base-pair long section of the DNA helix containing the dye molecule along with two nearby DNA helices. Next, using a set of custom translation and rotational transformations, we placed the dye molecules near the DNA helix to match the respective chemical structure. The bond between DNA and C6 conjugated dye molecules (ATTO 647N and Cy5) was created using the psfgen module of VMD. In sample 1 and 2, the dye molecules were connected to the backbone of the DNA whereas, in sample 3, it was connected to the thymine base.

The resulting systems were solvated with TIP3P water molecules<sup>72</sup> using the Solvate plugin of VMD.<sup>69</sup> Potassium, sodium, and chloride ions were added to produce the experimental buffer conditions (12.5 mM KCl and 2 M NaCl) using the autoionize plugin of VMD. Each final system measured  $9 \times 8 \times 9$  nm<sup>3</sup> and contained approximately 60 000 atoms (Figure S5a).

The assembled systems were subjected to energy minimization using the conjugate gradient method to remove the steric clashes between the solute and solvent. Following that, we equilibrated each system for 10 ns while harmonically restraining the C1' atoms of DNA using a spring constant of 1 kcal  $\text{mol}^{-1} \text{Å}^{-2}$ . Subsequently, we equilibrated the systems for an additional 10 ns with weaker harmonic restraints using a spring constant of 0.1 kcal mol<sup>-1</sup> Å<sup>-2</sup> while maintaining the hydrogen bonds between the complementary base-pairs of DNA using the extrabond utility of NAMD. Finally, we removed all the restraints (except the terminal C1' atoms of each DNA strand) and performed approximately 1  $\mu$ s long simulations of the systems using a constant number of atoms, pressure (P = 1 bar), and temperature (T = 298 K) ensemble. In order to mimic the connection of the DNA helices to the rest of the DNA origami plate, we harmonically restrained the terminal atoms of each DNA strand using a spring constant of 0.1 kcal  $\text{mol}^{-1}$  Å<sup>-2</sup>. Two sets of simulations were carried out for each design to improve sampling of the conformational space.

## **ASSOCIATED CONTENT**

### Supporting Information

The Supporting Information is available free of charge at https://pubs.acs.org/doi/10.1021/acsnano.0c10259.

Movie S1: 1  $\mu$ s long MD simulation trajectories of the ATTO 647N dye in sample 1 in the dye-conjugated DNA system (MPG)

Movie S2: 1  $\mu$ s long MD simulation trajectories of the ATTO 647N dye in sample 2 in the dye-conjugated DNA system (MPG)

Movie S3: 1  $\mu$ s long MD simulation trajectories of the ATTO 647N dye in sample 3 in the dye-conjugated DNA system (MPG)

Movie S4: 1  $\mu$ s long MD simulation trajectories of Cy5 in sample 1 in the dye-conjugated DNA system (MPG)

Movie S5: 1 µs long MD simulation trajectories of Cy5 in sample 2 in the dye-conjugated DNA system (MPG)

Linking chemistry of the ATTO 647N to DNA, data on the modulation, DNA-PAINT analysis, comparison of the orientation data for flipped and nonflipped populations, simulation data, and the DNA origami staple strands (PDF)

### **AUTHOR INFORMATION**

### **Corresponding Authors**

Fernando D. Stefani – Centro de Investigaciones en Bionanociencias (CIBION), Consejo Nacional de Investigaciones Científicas y Técnicas (CONICET), C1425FQD Ciudad Autónoma de Buenos Aires, Argentina; Departamento de Física, Facultad de Ciencias Exactas y Naturales, Universidad de Buenos Aires, C1428EHA Ciudad Autónoma de Buenos Aires, Argentina;

Email: fernando.stefani@df.uba.ar

Philip Tinnefeld — Department of Chemistry and Center for NanoScience, Ludwig-Maximilians-Universität München, 81377 München, Germany; orcid.org/0000-0003-4290-7770; Email: philip.tinnefeld@cup.uni-muenchen.de

Guillermo P. Acuna — Department of Physics, University of Fribourg, Fribourg CH-1700, Switzerland; ⊚ orcid.org/ 0000-0001-8066-2677; Email: guillermo.acuna@unifr.ch

### **Authors**

Kristina Hübner — Department of Chemistry and Center for NanoScience, Ludwig-Maximilians-Universität München, 81377 München, Germany; orcid.org/0000-0002-6476-5446

Himanshu Joshi — Department of Physics, University of Illinois at Urbana—Champaign, Urbana, Illinois 61801, United States; orcid.org/0000-0003-0769-524X

Aleksei Aksimentiev — Department of Physics, University of Illinois at Urbana—Champaign, Urbana, Illinois 61801, United States; Occid.org/0000-0002-6042-8442

Complete contact information is available at: https://pubs.acs.org/10.1021/acsnano.0c10259

# Notes

The authors declare no competing financial interest.

### **ACKNOWLEDGMENTS**

We thank Mario Raab for help with the wide-field setup and Florian Steiner for modification of the analysis software. H.J. and A.A. acknowledge support from the National Science Foundation (DMR-1827346). Computer time was provided through the Extreme Science and Engineering Discovery Environment (XSEDE) allocation MCA05S028 and the Leadership Resource Allocation MCB20012 on Frontera at Texas Advanced Computing Center. G.P.A. acknowledges support from the Swiss National Science Foundation (200021 184687) and from the ITN SuperCol funded by the European Union's Horizon 2020 research and innovation program under the Marie Skłodowska-Curie grant agreement 860914. P.T. acknowledges financial support by the BMBF (SIBOF, 03VP03891). This work was funded by the Deutsche Forschungsgemeinschaft (DFG, German Research Foundation) under German Excellence Strategy, EXC 2089/1-390776260 and INST 86/1904-1 FUGG, TI 329/9-2. F.D.S. is thankful for the financial support by CONICET, ANPCYT projects PICT2013-0792 and PICT-2014-0739, the Max-Planck-Society, and the Alexander von Humboldt Foundation.

### **REFERENCES**

- (1) Rothemund, P. W. K. Folding DNA to Create Nanoscale Shapes and Patterns. *Nature* **2006**, 440, 297–302.
- (2) Pilo-Pais, M.; Acuna, G. P.; Tinnefeld, P.; Liedl, T. Sculpting Light by Arranging Optical Components with DNA Nanostructures. *MRS Bull.* **2017**, 42 (12), 936–942.
- (3) Kuzyk, A.; Jungmann, R.; Acuna, G. P.; Liu, N. DNA Origami Route for Nanophotonics. *ACS Photonics* **2018**, *5* (4), 1151–1163.
- (4) Liu, N.; Liedl, T. DNA-Assembled Advanced Plasmonic Architectures. *Chem. Rev.* **2018**, *118* (6), 3032–3053.
- (5) Hentschel, M.; Schäferling, M.; Duan, X.; Giessen, H.; Liu, N. Chiral Plasmonics. Science Advances. 2017, 3 (5), 1–12.
- (6) Neubrech, F.; Hentschel, M.; Liu, N. Reconfigurable Plasmonic Chirality: Fundamentals and Applications. *Adv. Mater.* **2020**, 32 (41), 1905640.
- (7) Kuzyk, A.; Schreiber, R.; Fan, Z.; Pardatscher, G.; Roller, E. M.; Högele, A.; Simmel, F. C.; Govorov, A. O.; Liedl, T. DNA-Based Self-Assembly of Chiral Plasmonic Nanostructures with Tailored Optical Response. *Nature* **2012**, *483* (7389), 311–314.
- (8) Kuzyk, A.; Schreiber, R.; Zhang, H.; Govorov, A. O.; Liedl, T.; Liu, N. Reconfigurable 3D Plasmonic Metamolecules. *Nat. Mater.* **2014**, *13* (9), 862–866.
- (9) Huang, Y.; Nguyen, M.-K.; Natarajan, A. K.; Nguyen, V. H.; Kuzyk, A. A DNA Origami-Based Chiral Plasmonic Sensing Device. *ACS Appl. Mater. Interfaces* **2018**, *10* (51), 44221–44225.
- (10) Stein, I. H.; Steinhauer, C.; Tinnefeld, P. Single-Molecule Four-Color FRET Visualizes Energy-Transfer Paths on DNA Origami. *J. Am. Chem. Soc.* **2011**, *133* (12), 4193–4195.
- (11) Nicoli, F.; Barth, A.; Bae, W.; Neukirchinger, F.; Crevenna, A. H.; Lamb, D. C.; Liedl, T. Directional Photonic Wire Mediated by Homo-Förster Resonance Energy Transfer on a DNA Origami Platform. *ACS Nano* **2017**, *11*, 11264–11272.
- (12) Olejko, L.; Bald, I. FRET Efficiency and Antenna Effect in Multi-Color DNA Origami-Based Light Harvesting Systems. *RSC Adv.* **2017**, 7 (39), 23924–23934.
- (13) Dutta, P. K.; Varghese, R.; Nangreave, J.; Lin, S.; Yan, H.; Liu, Y. DNA-Directed Artificial Light-Harvesting Antenna. *J. Am. Chem. Soc.* **2011**, *133*, 11985–11993.
- (14) Selnihhin, D.; Sparvath, S. M.; Preus, S.; Birkedal, V.; Andersen, E. S. Multifluorophore DNA Origami Beacon as a Biosensing Platform. *ACS Nano* **2018**, *12*, 5699–5708.
- (15) Andersen, E. S.; Dong, M.; Nielsen, M. M.; Jahn, K.; Subramani, R.; Mamdouh, W.; Golas, M. M.; Sander, B.; Stark, H.; Oliveira, C. L. P.; Pedersen, J. S.; Birkedal, V.; Besenbacher, F.; Gothelf, K. V.; Kjems, J. Self-Assembly of a Nanoscale DNA Box with a Controllable Lid. *Nature* **2009**, 459, 73–76.
- (16) Kaminska, I.; Bohlen, J.; Mackowski, S.; Tinnefeld, P.; Acuna, G. P. Strong Plasmonic Enhancement of a Single Peridinin—Chlorophyll a Protein Complex on DNA Origami-Based Optical Antennas. *ACS Nano* **2018**, *12* (2), 1650—1655.
- (17) Kaminska, I.; Vietz, C.; Cuartero-González, Á.; Tinnefeld, P.; Fernández-Domínguez, A. I.; Acuna, G. P. Strong Plasmonic Enhancement of Single Molecule Photostability in Silver Dimer Optical Antennas. *Nanophotonics* **2018**, *7* (3), 643–649.
- (18) Vietz, C.; Kaminska, I.; Sanz Paz, M.; Tinnefeld, P.; Acuna, G. P. Broadband Fluorescence Enhancement with Self-Assembled Silver Nanoparticle Optical Antennas. *ACS Nano* **2017**, *11* (5), 4969–4975.
- (19) Prinz, J.; Heck, C.; Ellerik, L.; Merk, V.; Bald, I. DNA Origami Based Au–Ag-Core–Shell Nanoparticle Dimers with Single-Molecule SERS Sensitivity. *Nanoscale* **2016**, *8* (10), 5612–5620.
- (20) Simoncelli, S.; Roller, E.-M.; Urban, P.; Schreiber, R.; Turberfield, A. J.; Liedl, T.; Lohmüller, T. Quantitative Single-Molecule Surface-Enhanced Raman Scattering by Optothermal Tuning of DNA Origami-Assembled Plasmonic Nanoantennas. *ACS Nano* **2016**, *10* (11), 9809–9815.
- (21) Thacker, V. V.; Herrmann, L. O.; Sigle, D. O.; Zhang, T.; Liedl, T.; Baumberg, J. J.; Keyser, U. F. DNA Origami Based Assembly of Gold Nanoparticle Dimers for Surface-Enhanced Raman Scattering. *Nat. Commun.* **2014**, *5*, 3448.

- (22) Kühler, P.; Roller, E. M.; Schreiber, R.; Liedl, T.; Lohmüller, T.; Feldmann, J. Plasmonic DNA-Origami Nanoantennas for Surface-Enhanced Raman Spectroscopy. *Nano Lett.* **2014**, *14* (5), 2914–2919.
- (23) Bohlen, J.; Cuartero-González, Á.; Pibiri, E.; Ruhlandt, D.; Fernández-Domínguez, A. I.; Tinnefeld, P.; Acuna, G. P. Plasmon-Assisted Förster Resonance Energy Transfer at the Single-Molecule Level in the Moderate Quenching Regime. *Nanoscale* **2019**, *11* (16), 7674–7681.
- (24) Aissaoui, N.; Moth-Poulsen, K.; Käll, M.; Johansson, P.; Wilhelmsson, L. M.; Albinsson, B. FRET Enhancement Close to Gold Nanoparticles Positioned in DNA Origami Constructs. *Nanoscale* **2017**, *9* (2), 673–683.
- (25) Ojambati, O. S.; Chikkaraddy, R.; Deacon, W. D.; Horton, M.; Kos, D.; Turek, V. A.; Keyser, U. F.; Baumberg, J. J. Quantum Electrodynamics at Room Temperature Coupling a Single Vibrating Molecule with a Plasmonic Nanocavity. *Nat. Commun.* **2019**, *10* (1), 1049
- (26) Roller, E.-M.; Argyropoulos, C.; Högele, A.; Liedl, T.; Pilo-Pais, M. Plasmon–Exciton Coupling Using DNA Templates. *Nano Lett.* **2016**, *16*, 5962–5966.
- (27) Hübner, K.; Pilo-Pais, M.; Selbach, F.; Liedl, T.; Tinnefeld, P.; Stefani, F. D.; Acuna, G. P. Directing Single-Molecule Emission with DNA Origami-Assembled Optical Antennas. *Nano Lett.* **2019**, *19* (9), 6629–6634.
- (28) Raab, M.; Vietz, C.; Stefani, F. D.; Acuna, G. P.; Tinnefeld, P. Shifting Molecular Localization by Plasmonic Coupling in a Single-Molecule Mirage. *Nat. Commun.* **2017**, 8 (1), 13966.
- (29) Curto, A. G.; Volpe, G.; Taminiau, T. H.; Kreuzer, M. P.; Quidant, R.; Van Hulst, N. F. Unidirectional Emission of a Quantum Dot Coupled to a Nanoantenna. *Science* **2010**, 329 (5994), 930–933.
- (30) Pakizeh, T.; Käll, M. Unidirectional Ultracompact Optical Nanoantennas. *Nano Lett.* **2009**, *9*, 2343–2349.
- (31) Lakowicz, J. R. *Principles of Fluorescence Spectroscopy*, 3rd ed.; Springer US: Baltimore, 2006; pp 443–475.
- (32) Anger, P.; Bharadwaj, P.; Novotny, L. Enhancement and Quenching of Single-Molecule Fluorescence. *Phys. Rev. Lett.* **2006**, *96* (11), 113002.
- (33) Blanco, L. A.; García de Abajo, F. J. Spontaneous Emission Enhancement near Nanoparticles. *J. Quant. Spectrosc. Radiat. Transfer* **2004**, *89*, 37–40.
- (34) Rogobete, L.; Kaminski, F.; Agio, M.; Sandoghdar, V. Design of Plasmonic Nanoantennae for Enhancing Spontaneous Emission. *Opt. Lett.* **2007**, 32 (12), 1623–1625.
- (35) Mock, J. J.; Hill, R. T.; Degiron, A.; Zauscher, S.; Chilkoti, A.; Smith, D. R. Distance-Dependent Plasmon Resonant Coupling between a Gold Nanoparticle and Gold Film. *Nano Lett.* **2008**, 8 (8), 2245–2252.
- (36) Pal, S.; Deng, Z.; Wang, H.; Zou, S.; Liu, Y.; Yan, H. DNA Directed Self-Assembly of Anisotropic Plasmonic Nanostructures. *J. Am. Chem. Soc.* **2011**, *133* (44), 17606–17609.
- (37) Zhan, P.; Wen, T.; Wang, Z.; He, Y.; Shi, J.; Wang, T.; Liu, X.; Lu, G.; Ding, B. DNA Origami Directed Assembly of Gold Bowtie Nanoantennas for Single-Molecule Surface-Enhanced Raman Scattering. *Angew. Chem., Int. Ed.* **2018**, *57* (11), 2846–2850.
- (38) Ihmels, H.; Otto, D. Intercalation of Organic Dye Molecules into Double-Stranded DNA General Principles and Recent Developments. *Top. Curr. Chem.* **2005**, 258, 161–204.
- (39) Gopinath, A.; Thachuk, C.; Mitskovets, A.; Atwater, H. A.; Kirkpatrick, D.; Rothemund, P. W. K. Absolute and Arbitrary Orientation of Single Molecule Shapes. *Science* **2021**, *371* (6531), eabd6179.
- (40) Boulais, É.; Sawaya, N. P. D.; Veneziano, R.; Andreoni, A.; Banal, J. L.; Kondo, T.; Mandal, S.; Lin, S.; Schlau-Cohen, G. S.; Woodbury, N. W.; Yan, H.; Aspuru-Guzik, A.; Bathe, M. Programmed Coherent Coupling in a Synthetic DNA-Based Excitonic Circuit. *Nat. Mater.* **2018**, *17* (2), 159–166.
- (41) Loretan, M.; Domljanovic, I.; Lakatos, M.; Rüegg, C.; Acuna, G. P. DNA Origami as Emerging Technology for the Engineering of

- Fluorescent and Plasmonic-Based Biosensors. *Materials* **2020**, *13* (9), 2.185
- (42) Norman, D. G.; Grainger, R. J.; Uhrín, D.; Lilley, D. M. J. Location of Cyanine-3 on Double-Stranded DNA: Importance for Fluorescence Resonance Energy Transfer Studies. *Biochemistry* **2000**, 39 (21), 6317–6324.
- (43) Iqbal, A.; Arslan, S.; Okumus, B.; Wilson, T. J.; Giraud, G.; Norman, D. G.; Ha, T.; Lilley, D. M. J. Orientation Dependence in Fluorescent Energy Transfer between Cy3 and Cy5 Terminally Attached to Double-Stranded Nucleic Acids. *Proc. Natl. Acad. Sci. U. S. A.* 2008, 105 (32), 11176–11181.
- (44) Ranjit, S.; Gurunathan, K.; Levitus, M. Photophysics of Backbone Fluorescent DNA Modifications: Reducing Uncertainties in FRET. *J. Phys. Chem. B* **2009**, *113* (22), 7861–7866.
- (45) Cunningham, P. D.; Khachatrian, A.; Buckhout-White, S.; Deschamps, J. R.; Goldman, E. R.; Medintz, I. L.; Melinger, J. S. Resonance Energy Transfer in DNA Duplexes Labeled with Localized Dyes. *J. Phys. Chem. B* **2014**, *118* (59), 14555–14565.
- (46) Ouellet, J.; Schorr, S.; Iqbal, A.; Wilson, T. J.; Lilley, D. M. J. Orientation of Cyanine Fluorophores Terminally Attached to DNA *via* Long, Flexible Tethers. *Biophys. J.* **2011**, *101* (5), 1148–1154.
- (47) Mortensen, K. I.; Sung, J.; Flyvbjerg, H.; Spudich, J. A. Optimized Measurements of Separations and Angles between Intra-Molecular Fluorescent Markers. *Nat. Commun.* **2015**, *6* (1), 8621.
- (48) Backer, A. S.; Lee, M. Y.; Moerner, W. E. Enhanced DNA Imaging Using Super-Resolution Microscopy and Simultaneous Single-Molecule Orientation Measurements. *Optica* **2016**, 3 (6), 659.
- (49) Monneret, S.; Bertaux, N.; Savatier, J.; Shaban, H. A.; Mavrakis, M.; Valades Cruz, C. A.; Kress, A.; Brasselet, S. Quantitative Nanoscale Imaging of Orientational Order in Biological Filaments by Polarized Superresolution Microscopy. *Proc. Natl. Acad. Sci. U. S. A.* **2016**, *113* (7), E820–E828.
- (50) Jungmann, R.; Steinhauer, C.; Scheible, M.; Kuzyk, A.; Tinnefeld, P.; Simmel, F. C. Single-Molecule Kinetics and Super-Resolution Microscopy by Fluorescence Imaging of Transient Binding on DNA Origami. *Nano Lett.* **2010**, *10* (11), 4756–4761.
- (51) Vandenberk, N.; Barth, A.; Borrenberghs, D.; Hofkens, J.; Hendrix, J. Evaluation of Blue and Far-Red Dye Pairs in Single-Molecule Förster Resonance Energy Transfer Experiments. *J. Phys. Chem. B* **2018**, 122 (15), 4249–4266.
- (52) Kalinin, S.; Sisamakis, E.; Magennis, S. W.; Felekyan, S.; Seidel, C. A. M. On the Origin of Broadening of Single-Molecule FRET Efficiency Distributions beyond Shot Noise Limits. *J. Phys. Chem. B* **2010**, *114* (18), 6197–6206.
- (53) Wu, N.; Czajkowsky, D. M.; Zhang, J.; Qu, J.; Ye, M.; Zeng, D.; Zhou, X.; Hu, J.; Shao, Z.; Li, B.; Fan, C. Molecular Threading and Tunable Molecular Recognition on DNA Origami Nanostructures. *J. Am. Chem. Soc.* **2013**, *135* (33), 12172–12175.
- (54) Jungmann, R.; Avendaño, M. S.; Woehrstein, J. B.; Dai, M.; Shih, W. M.; Yin, P. Multiplexed 3D Cellular Super-Resolution Imaging with DNA-PAINT and Exchange-PAINT. *Nat. Methods* **2014**, *11* (3), 313–318.
- (55) Böhmer, M.; Enderlein, J. Orientation Imaging of Single Molecules by Wide-Field Epifluorescence Microscopy. *J. Opt. Soc. Am. B* **2003**, 20 (3), 554–559.
- (56) Koenderink, A. F. Single-Photon Nanoantennas. ACS Photonics 2017, 4 (4), 710–722.
- (57) Douglas, S. M.; Marblestone, A. H.; Teerapittayanon, S.; Vazquez, A.; Church, G. M.; Shih, W. M. Rapid Prototyping of 3D DNA-Origami Shapes with CaDNAno. *Nucleic Acids Res.* **2009**, 37 (15), 5001–5006.
- (58) Vogelsang, J.; Kasper, R.; Steinhauer, C.; Person, B.; Heilemann, M.; Sauer, M.; Tinnefeld, P. A Reducing and Oxidizing System Minimizes Photobleaching and Blinking of Fluorescent Dyes. *Angew. Chem., Int. Ed.* **2008**, *47* (29), 5465–5469.
- (59) Cordes, T.; Vogelsang, J.; Tinnefeld, P. On the Mechanism of Trolox as Antiblinking and Antibleaching Reagent. *J. Am. Chem. Soc.* **2009**, *131* (14), 5018–5019.

- (60) Edelstein, A.; Amodaj, N.; Hoover, K.; Vale, R.; Stuurman, N. Computer Control of Microscopes Using Manager. *Current Protocols in Molecular Biology.* **2010**, *92*, 14.20.1–14.20.17.
- (61) Phillips, J. C.; Hardy, D. J.; Maia, J. D. C.; Stone, J. E.; Ribeiro, J. V.; Bernardi, R. C.; Buch, R.; Fiorin, G.; Hénin, J.; Jiang, W.; McGreevy, R.; Melo, M. C. R.; Radak, B. K.; Skeel, R. D.; Singharoy, A.; Wang, Y.; Roux, B.; Aksimentiev, A.; Luthey-Schulten, Z.; Kale, L. V.; et al. Scalable Molecular Dynamics on CPU and GPU Architectures with NAMD. *J. Chem. Phys.* **2020**, *153*, 044130–1–33.
- (62) Batcho, P. F.; Case, D. A.; Schlick, T. Optimized Particle-Mesh Ewald/Multiple-Time Step Integration for Molecular Dynamics Simulations. *J. Chem. Phys.* **2001**, *115* (9), 4003–4018.
- (63) Feller, S. E.; Zhang, Y.; Pastor, R. W.; Brooks, B. R. Constant Pressure Molecular Dynamics Simulation: The Langevin Piston Method. *J. Chem. Phys.* **1995**, *103*, 4613–4621.
- (64) Miyamoto, S.; Kollman, P. A. Settle: An Analytical Version of the SHAKE and RATTLE Algorithm for Rigid Water Models. *J. Comput. Chem.* **1992**, *13* (8), 952–962.
- (65) Andersen, H. C. Rattle: A "Velocity" Version of the Shake Algorithm for Molecular Dynamics Calculations. *J. Comput. Phys.* **1983**, 52, 24–34.
- (66) Hart, K.; Foloppe, N.; Baker, C. M.; Denning, E. J.; Nilsson, L.; MacKerell, A. D. Optimization of the CHARMM Additive Force Field for DNA: Improved Treatment of the BI/BII Conformational Equilibrium. *J. Chem. Theory Comput.* **2012**, *8* (1), 348–362.
- (67) Vanommeslaeghe, K.; MacKerell, A. D. Automation of the CHARMM General Force Field (CGenFF) I: Bond Perception and Atom Typing, J. Chem. Inf. Model. 2012, 52 (12), 3144–3154.
- (68) Yoo, J.; Aksimentiev, A. Improved Parametrization of Li + , Na + , K + , and Mg 2+ Ions for All-Atom Molecular Dynamics Simulations of Nucleic Acid Systems. *J. Phys. Chem. Lett.* **2012**, 3 (1), 45–50.
- (69) Humphrey, W.; Dalke, A.; Schulten, K. VMD: Visual Molecular Dynamics. *J. Mol. Graphics* **1996**, *14* (1), 33–38.
- (70) Case, D. A.; Babin, V.; Berryman, J.; Betz, R. M.; Cai, Q.; Cerutti, D. S.; Cheatham, III, T. E.; Darden, T. A.; Duke, R. E.; Gohlke, H.; Goetz, A. W.; Gusarov, S.; Homeyer, N.; Janowski, P.; Kaus, J.; Kolossvary, I.; Kovalenko, A.; Lee, T. S.; LeGrand, S.; Luchko, T.; et al. *Manual AMBER 14*; University of California: San Francisco, 2014.
- (71) Yoo, J.; Aksimentiev, A. *In Situ* Structure and Dynamics of DNA Origami Determined through Molecular Dynamics Simulations. *Proc. Natl. Acad. Sci. U. S. A.* **2013**, *110* (50), 20099–20104.
- (72) Jorgensen, W. L.; Chandrasekhar, J.; Madura, J. D.; Impey, R. W.; Klein, M. L. Comparison of Simple Potential Functions for Simulating Liquid Water. *J. Chem. Phys.* **1983**, *79*, 926–935.